

Flux pinning in (1111) iron-pnictide superconducting crystals

C.J. van der Beek¹, G. Rizza¹, M. Konczykowski¹, P. Fertey², I. Monnet³, Thierry Klein⁴, R. Okazaki⁵, M. Ishikado⁶, H. Kito^{7,8}, A. Iyo^{7,8}, H. Eisaki^{7,8}, S. Shamoto^{6,8}, M.E. Tillman⁹, S.L. Bud'ko⁹, P.C. Canfield⁹, T. Shibauchi⁵, and Y. Matsuda⁵

¹Laboratoire des Solides Irradiés, CNRS UMR 7642 & CEA-DSM-IRAMIS, Ecole Polytechnique, 91128 Palaiseau, France

²Synchrotron SOLEIL, L'Orme des Merisiers, Saint-Aubin - BP 48, F-91192 Gif-sur-Yvette cedex, France

³CIMAP, 6 boulevard du Maréchal Juin, F-14050 Caen cedex 4, France

⁴Laboratoire Louis Néel, CNRS-UPR 5031, F-38042 Grenoble cedex, France

⁵Department of Physics, Kyoto University, Kyoto 606-8502, Japan

⁶Quantum Beam Science Directorate, Japan Atomic Energy Agency, Tokai, Naka, Ibaraki 319-1195, Japan

⁷Nanoelectronics Research Institute (NeRI), National Institute of Advanced Industrial Science and Technology (AIST), 1-1-1 Central 2, Tsukuba, Ibaraki 305-8568, Japan

⁸JST, Transformative Research-Project on Iron Pnictides (TRIP), Chiyoda-ku, Tokyo 102-0075

⁹Department of Physics & Astronomy and Ames Laboratory, Iowa State University, Ames, Iowa, U.S.A

(Dated: March 4, 2022)

Local magnetic measurements are used to quantitatively characterize heterogeneity and flux line pinning in PrFeAsO_{1-y} and NdFeAs(O,F) superconducting single crystals. In spite of spatial fluctuations of the critical current density on the macroscopic scale, it is shown that the major contribution comes from collective pinning of vortex lines by microscopic defects by the mean-free path fluctuation mechanism. The defect density extracted from experiment corresponds to the dopant atom density, which means that dopant atoms play an important role both in vortex pinning and in quasi-particle scattering. In the studied underdoped PrFeAsO_{1-y} and NdFeAs(O,F) crystals, there is a background of strong pinning, which we attribute to spatial variations of the dopant atom density on the scale of a few dozen to one hundred nm. These variations do not go beyond 5 % – we therefore do not find any evidence for coexistence of the superconducting and the antiferromagnetic phase. The critical current density in sub-T fields is characterized by the presence of a peak effect, the location of which in the (B, T) -plane is consistent with an order-disorder transition of the vortex lattice.

PACS numbers: 74.25.Sv; 74.25.Uv; 74.70.Xa ; 74.25.Wx ; 74.62.En

I. INTRODUCTION

The characterization of the physical properties of new superconducting materials such as the recently discovered iron-pnictide superconductors¹⁻⁷ requires a good knowledge of sample morphology and microstructure. The measurement and interpretation of thermodynamic quantities such as the magnetization, the magnetic torque,¹⁰ or the specific heat, or transport properties such as the resistance or irreversible magnetization, may be complicated by material inhomogeneity on mesoscopic or macroscopic length scales. On the other hand, microscopic disorder is well-known to be beneficial for vortex line pinning and high critical currents. Finally, from the defect-vortex interaction, one might hope to extract information on electronic scattering mechanisms in the iron-pnictide superconductors, as well as on the premise of phase co-existence. In underdoped pnictides especially, it has been argued that the coexistence of the low-doping anti-ferromagnetic state and the superconducting state at higher doping levels may affect physical properties.⁹

Vortex pinning and the critical current density in the iron pnictide superconductors has mainly focussed on the so-called “122” compounds, since large single crystals of these are available. Most notably, magnetic flux penetration in $\text{Ba}(\text{Fe}_{0.93}\text{Co}_{0.07})_2\text{As}_2$ has been studied using magneto-optical imaging by Prozorov *et al.*^{11,12} The

same authors reported on the irreversible magnetization and flux creep in this compound, and found qualitative agreement with collective creep in the so-called bundle regime.¹³ The non-monotonous behavior of the sustainable current as function of magnetic field was interpreted in terms of a crossover to plastic creep.¹¹ A similar behavior was found for crystals with different doping levels;^{12,14} the overall behavior of the critical current density as function of doping was attributed to the changing density of structural domain walls, that act as strong pinning centers.¹⁵ Yamamoto *et al.* obtained similar results on the same $\text{Ba}(\text{Fe}_{0.9}\text{Co}_{0.1})_2\text{As}_2$, but attributed the temperature- and field-dependent features of the critical current density to an inhomogeneous distribution of Co atoms.¹⁶ Very large critical currents, as well as a non-monotonous width of the irreversible magnetization loops corresponding to a peak-effect in the critical current¹⁷⁻²¹ were measured by Yang *et al.* in single crystalline $\text{Ba}_{0.6}\text{K}_{0.4}\text{Fe}_2\text{As}_2$,²² who concluded to the presence of small-sized normal state regions in their samples. Finally, irreversible magnetization and flux creep measurements were conducted on $\text{SmFeAsO}_{0.9}\text{F}_{0.1}$ ²³ and polycrystalline $\text{NdFeAsO}_{0.82}\text{Fe}_{0.18}$,^{24,25} members of the “1111” family of compounds. In all the above cases, the critical current at low fields was characterized by a peak and negligible magnetic relaxation, followed by more pronounced thermally activated flux motion at higher fields,

which was found to be in qualitative agreement with the collective creep theory.¹³ However, no quantitative analysis of the data has been performed, and no definite consensus as to the defects at the origin of flux pinning has been established.

The aim of the present paper is the identification of defects responsible for flux pinning in single crystals of the (Re)FeAsO “1111” family of superconducting compounds. The microstructure is characterized by the undulation of the FeAs layers and the presence of sparse nanometer-sized defects, both of which do not seem to influence flux pinning. The largest contribution to the critical current j_c is shown to arise from the dopant atoms, which act as scatterers for quasi-particles in the vortex cores. One therefore deals with pinning by local variations of the mean-free path ($\delta\kappa$ mechanism). The temperature- and field dependence of j_c is very well described by collective flux pinning in the single-vortex limit, but superposed on a strong pinning contribution arising from small fluctuations of the doping level on the scale of dozens of nm.

II. EXPERIMENTAL DETAILS

PrFeAsO_{1-y} crystals (with the P4/mmm structure) were grown at 1300°C and 2 GPa from pressed pellets consisting of the starting materials PrAs, Fe, and Fe₂O₃, in the nominal composition PrFeAsO_{0.6}.^{26,27} The typical size of the crystals is $100 \times 100 \times 30 \mu\text{m}^3$; the average final composition corresponds to $y \sim 0.1$. A number of monolithic crystals from this batch has been previously used for the measurement of the superfluid density,²⁸ the field of first flux penetration,²⁷ and the electrical resistivity in the vicinity of the upper critical field $B_{c2} = \Phi_0/2\pi\xi^2$ (with ξ the coherence length).²⁷ The superconducting properties of the compound are therefore completely characterized. The temperature dependence of the in-plane penetration depth $\lambda_{ab}(T)$ (for currents parallel to the ab plane) is well described by a simple two-gap model, without any nodes of the order parameter. The magnitude of the low temperature penetration depth is $\lambda_{ab}(0) = 280 \text{ nm}$.²⁷ Table I gathers the superconducting parameters of PrFeAsO_{1-y}, including the characteristic energy $\varepsilon_0 \equiv \Phi_0^2/4\pi\mu_0\lambda_{ab}^2$ (corresponding to $4\xi^2$ times the condensation energy), the low-field anisotropy ratio $\varepsilon_\lambda \equiv \lambda_{ab}/\lambda_c$, and the depairing current $j_0 \equiv 4\varepsilon_0/\sqrt{3}\Phi_0\xi$ ($\mu_0 \equiv 4\pi \times 10^{-7} \text{ Hm}^{-1}$).

Several PrFeAsO_{1-y} crystals were prepared for Transmission Electron Microscopy (TEM). In each case, two crystals, of lateral dimensions $\sim 100 \mu\text{m}$, were glued between 0.5 mm thick Si platelets; these were then thinned down until the crystals were flush with the edges. Further thinning yielded sections parallel to the c -axis, suitable for TEM. Figure 1a, a high resolution image of one of the sections, shows clear contrast corresponding to the FeAs planes, with some undulation. The presence of 5 - 10 nm sized defects, possibly secondary phase precipitates, is

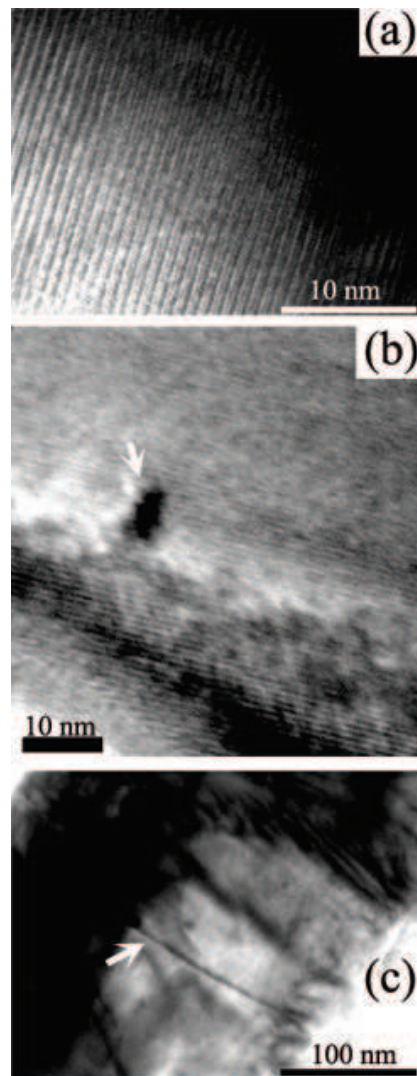


FIG. 1: Transmission electron microscopy images of single crystalline PrFeAsO_{1-y} (a) High resolution bright field image, revealing the undulation of the FeAs layers. (b) Bright field micrograph of a zone containing a nm-size inclusion (indicated by the white arrow). (c) Bright field image revealing contrast due to a line dislocation (indicated by the arrow).

also observed (Fig. 1b). These defects are separated by a distance of the order of several dozen to several hundred nm, depending on location. Finally, Fig. 1 shows contrast associated with the presence of a linear dislocation core, occasional examples of which were found.

Three PrFeAsO_{1-y} crystals (# 1, 3, and 7) were characterized by X-ray diffraction using 28.3 keV (0.43811 Å) radiation on the CRISTAL beam at the SOLEIL synchrotron. Images of diffraction spots were collected on a 2D CCD detector when the sample was rotated around an axis in the ab plane. From the 360 measured images, successively collected during 1 s after a progression of 1° of the crystal rotation, layers of reciprocal space were numerically reconstructed. Three such sections, contain-

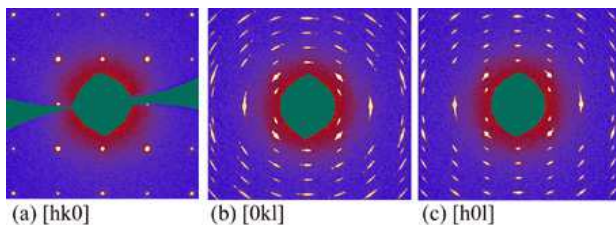


FIG. 2: (color online) Cuts through reciprocal space of the PrFeAsO_{1-y} compound, reconstructed from synchrotron radiation X-ray diffraction on crystal # 7 (the same crystal as in Ref.²⁷). (a) the $[\text{hk}0]$ plane (b) the $[0\text{kl}]$ plane; (c) the $[\text{h}0\text{l}]$ plane.

ing the origin, are shown in Fig. 2. The $[\text{hk}0]$ section reveals very good translational order in the basal plane. However, the fulfilment of the Laue condition over extended streaks in the $[\text{h}0\text{l}]$ and $[0\text{kl}]$ planes shows that crystalline order along the c -axis is not as good. The pronounced elongation of both low- and higher order nodes in the $[00\text{l}]$ direction indicates that this disorder more than likely originates from the undulation of the planes observed in TEM. Other kinds of c -axis disorder such as stacking faults or anti-phase boundaries would have yielded a larger broadening of nodes outside the $[\text{hk}0]$ plane, as compared to the lower order nodes. From the elongation of the nodes at $[100]$ and $[010]$, we estimate the buckling of the layers to result in a variation of their orientation of up to 5° . The same results were obtained for all studied crystals.

The $\text{NdFeAsO}_{0.9}\text{F}_{0.1}$ crystals used in this study are the same as that of Ref. 29; they were synthesized at high pressure in a cubic, multi-anvil apparatus. The crystals, extracted from a polycrystalline batch, had dimensions $210 \times 320 \times 30 \mu\text{m}^3$ (# 1) and $150 \times 200 \times 50 \mu\text{m}^3$ (# 2), and critical temperatures $T_c = 34.5 \pm 1.5 \text{ K}$ (# 1) and $37.5 \pm 1 \text{ K}$ (# 2). The superconducting parameters of $\text{NdFeAs}(\text{O},\text{F})$ of this particular doping level have been studied in Refs. 29 and 30, and are summarized in Table I.

In order to obtain the value and local distribution of T_c and j_c , flux penetration into the superconducting crystals was imaged using the direct magneto-optical imaging (MOI) method.³¹ Crystalline inhomogeneity in the vicinity of the critical temperature was characterized using the Differential Magneto-Optical (DMO) method.³² In MOI, a ferrimagnetic garnet indicator with in-plane anisotropy is placed on top of the sample under study, and observed using a polarized light microscope. The presence of a non-zero perpendicular component B_\perp of

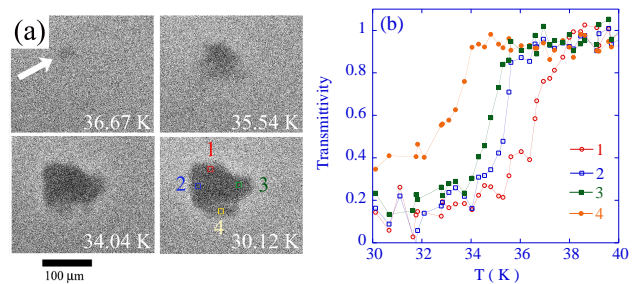


FIG. 3: (color online) (a) DMO images of the screening of an ac field of 1 Oe by PrFeAsO_{1-y} (b) crystal # 1, at various temperatures close to T_c . Screening first appears in the upper left-hand corner by the crystal (indicated by the arrow). The crystal progressively transits to the superconducting state between 38 and 32 K. (b) Local permeability, defined as the ratio $(I(\mathbf{r}, T) - I(\mathbf{r}, T \ll T_c)) / (I(\mathbf{r}, T \gg T_c) - I(\mathbf{r}, T \ll T_c))$ of the local luminous intensities $I(\mathbf{r}, T)$, in the zones 1–4 indicated in (a).

the magnetic induction is revealed, by virtue of the Faraday effect of the garnet, as a non-zero intensity of reflected light when the polarizers of the microscope are (nearly) crossed. Thus, light areas in the MO images correspond to areas of high perpendicular induction, while dark regions have small or zero B_\perp . In DMO, magneto-optical images taken at applied fields H_a and $H_a + \Delta H_a$ (with $\Delta H_a = 1 \text{ Oe}$) are subtracted; the procedure is repeated 100 times, and the subtracted images averaged.

The local critical current density of the investigated crystals was obtained by calibrating the luminous intensity of the MOI images, so as to obtain a map of the local induction. j_c was then determined as twice the gradient of the local flux density, measured over an interval of length $20 \mu\text{m}$ perpendicular to the sample boundary, and averaged over a width of $20 \mu\text{m}$, (parallel to the sample boundary). This procedure is justified in that, given our crystals' aspect ratio, flux profiles at the sample surface are nearly linear.³³ In what follows, the area over which j_c was measured was chosen such that $\langle B \rangle \approx 300 \text{ Oe}$ over the $20 \times 20 \mu\text{m}^2$ region.

Further measurements were carried out using a micron-sized Hall probe array, tailored in pseudomorphic $\text{GaAlAs}/\text{GaAs}$ heterostructure.^{27,34} The 10 Hall sensors of the array had an active area of $3 \times 3 \mu\text{m}^2$, while an eleventh sensor was used for the measurement of the applied field. The Hall probe magnetometry technique is complementary to magneto-optical imaging in that it has greater sensitivity and can be used up to substantially higher magnetic fields; on the other hand, it only allows the measurement of B_\perp along the array of sensors, and not over the entire two-dimensional sample surface.

compound	$\lambda_{ab}(0)$	$\varepsilon_\lambda(0)$	$\xi_{ab}(0)$	$\varepsilon_0(0)$	$j_0(0)$	Gi
$\text{PrFeAsO}_{0.9}$ ²⁷	280 nm	0.4	1.8 nm	$3.2 \times 10^{-12} \text{ Jm}^{-1}$	$2 \times 10^{12} \text{ Am}^{-2}$	3×10^{-3}
$\text{NdFeAsO}_{0.9}\text{F}_{0.1}$ ^{29,30}	$270 \pm 40 \text{ nm}$	0.25	2.4 nm	$3.5 \times 10^{-12} \text{ Jm}^{-1}$	$1.6 \times 10^{12} \text{ Am}^{-2}$	3×10^{-3}

TABLE I: Superconducting properties of the crystals used in this study.

III. RESULTS

A. PrFeAsO_{1-y}

Spatial inhomogeneity of the critical temperature in single crystals was investigated by the DMO images near the transition. A typical example is shown in Fig. 3a, depicting four DMO images, acquired with a $\Delta H_a = 1$ Oe modulation in the absence of a static field, at various temperatures spanning the normal-to-superconducting transition. In this particular case, diamagnetic screening first appears at $T \sim 38$ K in the upper left-hand corner of the crystal. Magnetic flux is progressively excluded from the crystal bulk, until the largest part is fully screened at $T = 34$ K. However, the small grain at the bottom is only fully screening at $T = 31$ K. Fig. 3b shows the ac permeability, determined from the luminous intensities $I(\mathbf{r}, T)$ as $T_{MO} = (I(\mathbf{r}, T) - I(\mathbf{r}, T \ll T_c)) / (I(\mathbf{r}, T \gg T_c) - I(\mathbf{r}, T \ll T_c))$, for four regions indicated in the last panel of Fig. 3a. It is seen that, locally, the crystal shows sharp transitions to the superconducting state. However, a global measurement (*e.g.* by a commercial magnetometer) would clearly result in a broadened transition.

Local values of the critical current density j_c are obtained from the MO imaging of the largest grains in polycrystalline conglomerates, or from the flux distribution in monolithic crystals, such as depicted in 4a, for PrFeAsO_{1-y} crystal # 7. The magnetic flux distributions in such crystals are characteristic of the Bean critical state;^{33,35-37} Fig. 4 shows an example of profiles obtained across the central part of crystal # 7 at $T = 11$ K. Due to the relatively large thickness-to-width ratio of the crystal, $d/w \sim 0.3$, flux profiles resemble straight lines; $j_c \approx \frac{1}{2} dB_{\perp} / dx$ can be straightforwardly obtained from the flux density gradient.³³

Resulting values of the critical current density in four areas of PrFeAsO_{1-y} crystal # 7 are shown in Fig. 5, as function of temperature. The inset to the Figure reveals the inhomogeneity of T_c for this particular crystal; the regions in which j_c was measured are also indicated. It is found that $j_c = 3 \pm 1 \times 10^9$ Am⁻² at the lowest measured temperature. The temperature dependence $j_c(T)$ depends on location. Low j_c areas show a smooth decrease with temperature, whereas regions where j_c is higher feature a crossover in the temperature dependence. Similar behavior is found in all investigated PrFeAsO_{1-y} crystals, see Fig. 6. We shall, in section IV, attribute this behavior to the additive effect of weak collective pinning by oxygen dopant atoms, yielding a strong temperature dependence, and strong pinning, with a weak temperature dependence, coming from disorder of the doping level on the scale of 10 - 100 nm .

Measurements in higher magnetic fields were performed using the Hall array magnetometry technique. Typical results for the self-field, defined as $H_s = B_{\perp} / \mu_0 - H_a$, measured on the central part of the top surface of crystal # 7, are shown in Fig. 7. The screening current density is proportional to the difference ΔH_s mea-

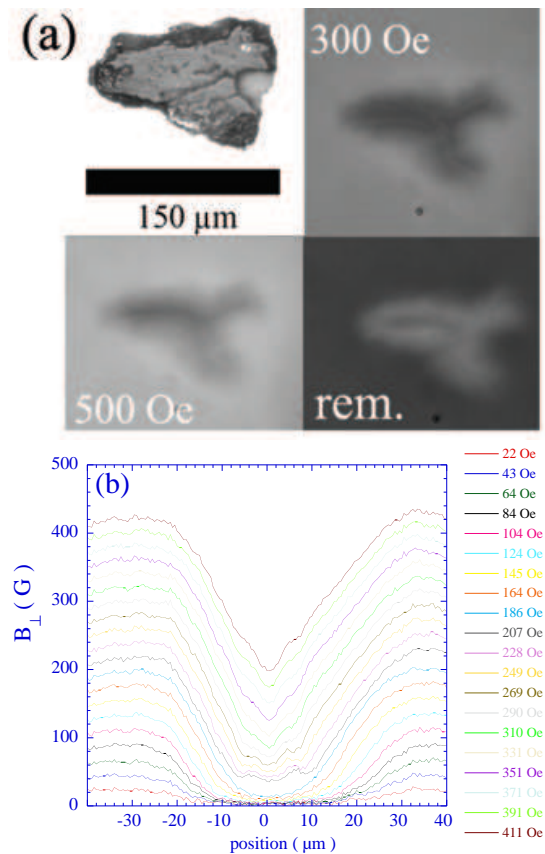


FIG. 4: (color online) (a) Direct MOI of the screening of a dc field by PrFeAsO_{1-y} crystal # 7 (the same crystal as in Ref.²⁷), at 7.1 K. Shown are a polarized light image of the crystal; and MOI for $H_a = 300$ Oe, 500 Oe, and the trapped flux in zero field (after the application of 500 Oe). (b) Flux profiles, measured from top to bottom across the central part of this crystal, for increasing values of the applied magnetic field H_a , and a temperature of 11 K.

sured on the decreasing- and increasing field branches, respectively. A clearly non-monotonous field-dependence of the critical current is observed, with the sustainable current density j rapidly decreasing as the H_a is first increased, followed by an intermediate regime of constant j . Fig. 11(a) shows that the low-field behavior, a plateau up to B^* , followed by a power-law decrease $\sim B^{-5/8}$, is archetypal for a strong pinning contribution to the critical current. However, at intermediate fields, around 0.1 T in Fig. 11(a), j_c does not vanish, but saturates at a value $j_c^{SV} \sim 2 - 3 \times 10^9$ Am⁻² at low temperature. The temperature dependence of the zero-field- and intermediate (constant) values of the critical current are plotted in Fig. 6. One sees that the j_c^{SV} contribution is spatially rather more homogeneous, and also that it corresponds to the critical current measured in the most weakly pinning areas of the crystals. Below, we shall attribute this contribution to weak collective pinning by dopant atoms. The strong pinning contribution $j_c(0)$ strongly depends on the location at which it is measured, and it is respon-

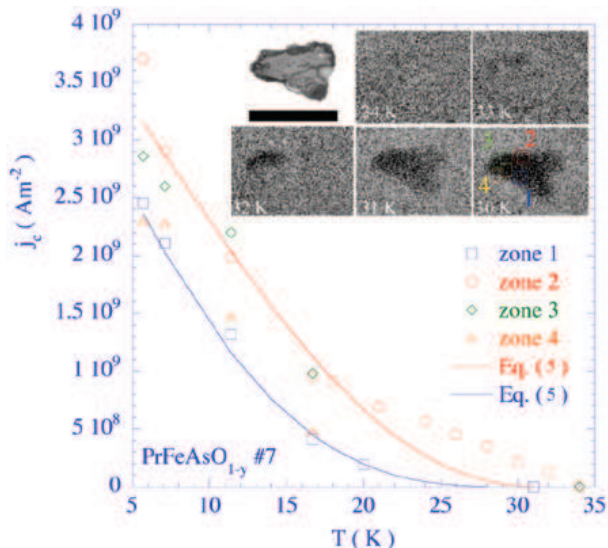


FIG. 5: (color online) Critical current density j_c of PrFeAsO_{1-y} crystal 7 at $H_a = 300$ Oe, as function of temperature. j_c was determined from the slope of the local magnetic flux density, measured in the different regions of the crystal indicated in the Inset. The lower drawn line is a fit to Eq. (5), with $n_d = 1.5 \times 10^{27} \text{ m}^{-3}$, the upper drawn line shows that the low temperature $j_c(T)$ in the strongly pinning regions is the same. Inset: Polarized light image of the crystal, and five DMO images of screening of $\Delta H_a = 1$ Oe at $T = 34 - 30$ K (in steps of -1 K). The regions 1 – 4 over which j_c was determined are indicated by drawn squares.

sible for the larger measured critical current densities.

Finally, we turn to higher applied magnetic fields. It is observed that the hysteresis loops open up at a field B_{on} , corresponding to the increase of j at the so-called “fishtail” or peak-effect.^{11,14,17,20–23,25} The $B_{on}(T)$ data are collected, together with the irreversibility fields determined from the appearance of a third harmonic component in the ac-response³⁸, in Fig. 12.

As in previous studies on other iron pnictide superconductors,^{11,14,22,23,25} the local flux density in Tesla fields is observed to decay with time, with a typical relaxation rate $S = (d \ln B_{\perp} / d \ln t) \sim -0.05$ for fields below H_{on} and $S \sim -0.03$ for $H_a > H_{on}$. As in other studies,¹⁴ magnetic relaxation was not observed to affect the low-field MO data. it therefore does not affect the measured temperature dependence of the critical current density in what follows.

B. $\text{NdFeAsO}_{1-x}\text{F}_x$

Fig. 8a shows magneto-optical images of flux penetration into $\text{NdFeAsO}_{0.9}\text{F}_{0.1}$ crystal # 1. The sample turns out to be a bicrystal, with a similar spread in T_c as observed in PrFeAsO_{1-y} . As shown by Fig. 8b, flux distributions inside the crystalline grains are well-described by the Bean critical state model.³³ Local values of the

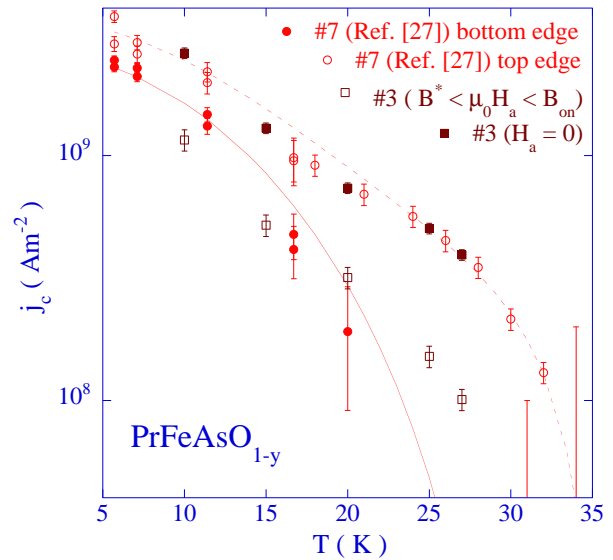


FIG. 6: (color online) PrFeAsO_{1-y} : critical current versus temperature, for two different crystals. Open and closed circles represent the upper and lower bounds of the j_c of crystal #7,²⁷ the closed squares represent the zero-field j_c of crystal #3, while the open squares depict the magnitude of the critical current in the field regime between B^* , above which the strong pinning contribution becomes negligible, but below the onset field of the “fishtail” effect, B_{on} . This value of j_c is attributed to weak collective pinning by oxygen vacancies in the single vortex limit; the drawn line represents a fit to Eq. (5), with $n_d = 1.5 \times 10^{27} \text{ m}^{-3}$. The dashed line is a fit to Eq. (10) summing strong and weak pinning contributions to the critical current at zero field, with parameter values $n_d = 1.5 \times 10^{27} \text{ m}^{-3}$, $n_i = 1 \times 10^{21} \text{ m}^{-3}$, and $f_{p,s} = 0.1\epsilon_0$.

critical current density at $B_{\perp} \approx 300$ Oe were obtained in the same manner as described above. Results for the three regions outlined in the center panel of Fig. 8a are rendered as function of temperature in Fig. 9, together with results obtained by Hall probe magnetometry over the central regions of crystals #1 and 2. Field-dependent results are shown in fig. 11(b). The overall behavior recalls that reported in Ref. 25, and is very similar to that observed in PrFeAsO_{1-y} : high critical current areas correspond to a large local contribution of strong pinning, whereas the lower j_c^{SV} measured at intermediate fields much above B^* corresponds to the critical current density in the more weakly pinning areas of the crystals. In contrast to PrFeAsO_{1-y} , the strong pinning contribution outweighs j_c^{SV} by a factor 2–3. $\text{NdFeAsO}(\text{O},\text{F})$ crystal # 2 shows a clear “fishtail” or peak-effect, the corresponding $B_{on}(T)$ values are plotted in Fig. 12. A hint of a peak-effect is also observed in crystal # 1, but the relative increase of the sustainable current density is much more modest than in the other investigated samples, with data resembling those of Ref. 25. Finally, Fig. 12 shows that the irreversibility field measured from the onset of screening²⁹ coincides with that determined

from the onset of a third harmonic response in ac Hall-probe array magnetometry. Moreover, the irreversibility field $B_{irr}(T)$ for NdFeAs(O,F) and PrFeAsO_{1-y} crystals with the same T_c are, within experimental accuracy, identical.

IV. DISCUSSION

A. Weak collective pinning

We start by analyzing the critical current contribution j_c^{SV} in terms of the weak collective pinning theory.^{13,39,40} The vortex lattice order is characterized by the transverse and longitudinal displacement correlation lengths

$$\langle |\mathbf{u}(R_c, z) - \mathbf{u}(0, z)|^2 \rangle = r_p^2 \quad (1)$$

$$\langle |\mathbf{u}(\mathbf{r}, L_c) - \mathbf{u}(\mathbf{r}, 0)|^2 \rangle = r_p^2. \quad (2)$$

where $\mathbf{u}(\mathbf{r}, z)$ denotes the deformation field of the vortex lattice at position (\mathbf{r}, z) (with $z \parallel \mathbf{B}$), and $r_p \sim \xi$ is the range of the pinning potential.⁴¹ The transverse displacement correlation length

$$R_c = \left(\frac{\varepsilon_0 \xi}{2\Phi_0 j_c} \right)^{1/2} \quad (3)$$

can be obtained, without a priori assumptions, from the value of the critical current density. Using the appropriate parameters (Table I), one has, for $j_c^{SV}(5\text{ K}) = 3 \times 10^9 \text{ Am}^{-2}$, $R_c = 40 \text{ nm}$ in single crystalline PrFeAsO_{1-y}, and $R_c = 56 \text{ nm}$ corresponding to $j_c^{SV}(5\text{ K}) \sim 1 \times 10^9 \text{ Am}^{-2}$

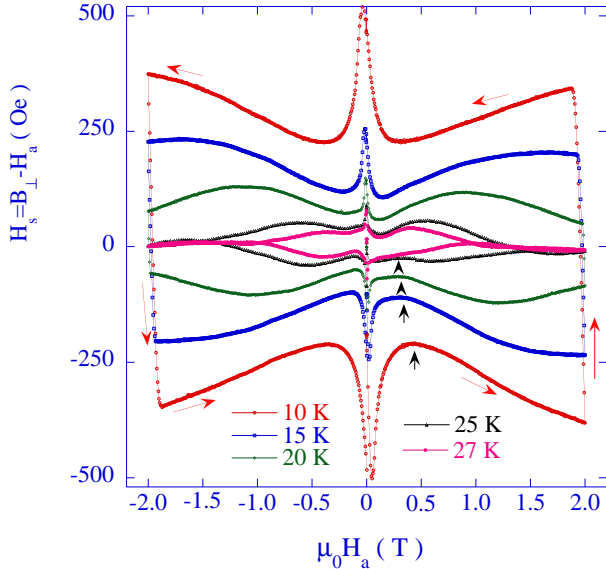


FIG. 7: (color online) Hysteresis loops of the “self-field”, defined as $H_s = B_{\perp}/\mu_0 - H_a$, as measured with a microscopic Hall sensor in the center of PrFeAsO_{1-y} crystal # 7, at the indicated temperatures. The values of the onset field H_{on} are denoted by the vertical black arrows.

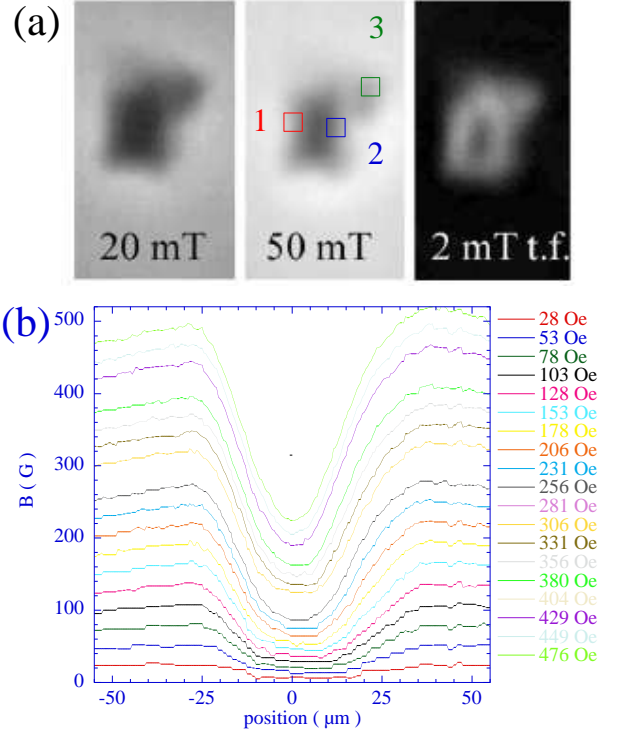


FIG. 8: (color online) (a) MOI flux penetration into NdFeAsO_{0.9}F_{0.1} crystal # 1, at $T = 9.1 \text{ K}$. The three frames depict the flux density distribution after the application of an applied field of 20 and 50 mT, and the remanent flux after removal of the 50 mT applied field. (b) Flux density profiles measured across the central part of the crystal.

in NdFeAsO_{0.9}F_{0.1}. These values are much smaller than the intervortex spacing at 300 Oe, at which the data in Figs. 5, 6, and 9 were obtained. The pinning-induced displacement of each vortex is thus independent of that of neighboring vortices. In this so-called single vortex pinning limit, one may now estimate the longitudinal displacement correlation length as

$$L_c = \xi \left(\frac{\sqrt{3}\varepsilon_\lambda^2 \varepsilon_0}{2j_c \Phi_0 \xi} \right)^{1/2}; \quad (4)$$

one finds $L_c \approx 20 \text{ nm}$ and 10 nm for PrFeAsO_{1-y} and NdFeAsO_{0.9}F_{0.1}, respectively. This length largely exceeds the spacing of the FeAs planes, which clearly establishes pinning as being in the three-dimensional single-vortex (3DSV) limit.^{13,40}

From here on, we show that the critical current density in the (1111) iron oxypnictide superconductors can be understood as arising from mean-free path variations induced by the dopant atoms, oxygen vacancies in the case of PrFeAsO_{1-y}, and F ions in the case of NdFeAsO_{0.9}F_{0.1}. The pinning force of a single defect is expressed as $f_p \sim 0.3g(\rho_D)\varepsilon_0 (\sigma_{tr}/\pi\xi^2) (\xi_0/\xi)$, where $\sigma_{tr} = \pi D_v^2$ is the transport scattering cross-section, D_v is the effective ion radius, and $g(\rho_D)$ is the Gor'kov function. The disorder parameter $\rho_D = \hbar v_F/2\pi T_c l \sim \xi_0/l$,

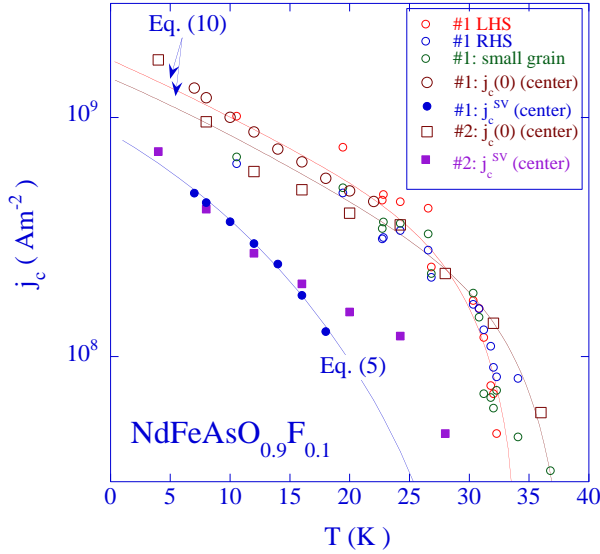


FIG. 9: (color online) Local values of the critical current density j_c in the three regions of the $\text{NdFeAsO}_{0.9}\text{F}_{0.1}$ crystal #1, outlined in the central panel of 9a. Also shown are the values of j_c^{SV} and $j_c^s(0)$ determined for both investigated crystals. The first are compared to Eq. (5) using $n_d = 1.5 \times 10^{27} \text{ m}^{-3}$ and $D_v = 0.9 \text{ nm}$ (lower drawn line), while the latter are fit to Eq. (10) with respective parameter sets ($T_c = 37 \text{ K}$, $n_i = 6 \times 10^{21} \text{ m}^{-3}$, $f_{p,s} = 0.1\epsilon_0$) and ($T_c = 35 \text{ K}$, $n_i = 2 \times 10^{22} \text{ m}^{-3}$, $f_{p,s} = 0.1\epsilon_0$).

with v_F the Fermi velocity, l the mean free path, and $\xi_0 \approx 1.35\xi(0)$ the (temperature-independent) Bardeen-Cooper-Schrieffer coherence length.^{13,42} The critical current is determined by the fluctuation of the elementary pinning force, $\langle f_p^2 \rangle$, and reads⁴³

$$j_c^{SV} \approx j_0 \left[\frac{0.1n_d D_v^4}{\epsilon_\lambda \xi} \left(\frac{\xi_0}{\xi} \right)^2 \right]^{2/3} \quad (5)$$

$$\propto \left[\frac{\lambda(0)}{\lambda(T)} \right]^2 \left(1 - \frac{T}{T_c} \right)^\alpha. \quad (6)$$

The numerical factor under the parentheses in Eq. (5) depends on the precise type of scattering.⁴² Since the temperature dependences $\lambda(0)/\lambda(T)$ and $\epsilon_\lambda(T)$ are known from Refs. 27 and 30 (yielding $\alpha \sim 2$ for PrFeAsO_{1-y} and $\alpha \sim 1.5$ for $\text{NdFeAsO}_{0.9}\text{F}_{0.1}$), one is in the position where a full consistency check of both the magnitude and the temperature dependence of j_c is possible.⁴⁴

In the case of PrFeAsO_{1-y} , Eq. (5), we start from the hypothesis that O vacancies are responsible for the lion's share of flux pinning. The ion radius $D_v = 1.46 \times 10^{10} \text{ m}$. Inserting this value into Eq. 5 reproduces the low-temperature value $j_c^{SV} = 3 \times 10^9 \text{ Am}^{-2}$ with the single free parameter $n_d \approx 1.5 \times 10^{27} \text{ m}^{-3}$. This nicely corresponds to 0.1 O vacancy per formula unit (half a unit cell of volume 65 \AA^3). Eq. (5) reproduces the low- T temperature dependence of the critical current density

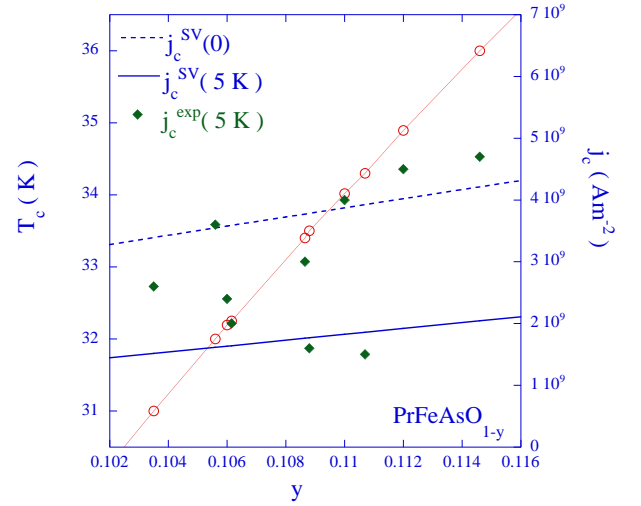


FIG. 10: (color online) PrFeAsO_{1-y} : critical current versus doping level, as determined from the phase diagram of Ref. 45. Open circles indicate the critical temperature, filled diamonds indicate the critical current density as measured in various locations in the four different crystals of Fig. 6. The dashed and drawn lines indicate the critical current density expected from weak collective pinning by oxygen vacancies, Eq. (5), at $T = 0$ and $T = 5 \text{ K}$, respectively (here we suppose that $\lambda_{ab}^{-2} \propto T_c$, as in Ref. 47).

in the high- j_c regions, and the temperature dependence over the full range from 5 K to T_c in the low- j_c regions. The spatially more homogeneous contribution to the critical current density of oxygen deficient single crystalline PrFeAsO_{1-y} is therefore well-described by pinning by O-vacancies by the $\delta\kappa$ mechanism.

In the case of $\text{NdFeAsO}_{0.9}\text{F}_{0.1}$, the analysis is hindered by our ignorance of the effective scattering cross-section: doping is through chemical substitution, not oxygen depletion. If one adopts the view that F substitution is at the origin of pinning, one has $n_d \sim 1.5 \times 10^{27} \text{ m}^{-3}$ for our average doping level. To reproduce the value of the measured low- T $j_c \approx 1 \times 10^9 \text{ Am}^{-2}$ then requires $\sigma_{tr} = 1.5 \times 10^{-20} \text{ m}^2$, corresponding to an effective defect radius of 0.9 \AA (this can be compared to the F ion radius of 1.3 \AA). The temperature dependence of j_c^{SV} is again very well described by Eq. (5). It is not quite as strong as in PrFeAsO_{1-y} , an effect that can be attributed to the different T -dependence of the penetration depth [$\lambda(T)$ nearly perfectly follows $\lambda^{-2} \sim (1 - t^2)$] and of the anisotropy ratio (ϵ_λ seems to be nearly independent of temperature in $\text{NdFeAs}_{0.9}\text{F}_{0.1}$).³⁰

B. Spatial variations of j_c and link with doping

Both investigated (1111) compounds show spatial variations of both the critical temperature T_c and the low-temperature critical current density j_c . It is tempting to correlate the two: knowing the temperature dependence

of both the superfluid density λ^{-2} and the anisotropy ratio, as well as the evolution of the respective T_c vs. doping phase diagrams^{4,45}, Eq. (5) predicts what the dependence $j_c(T_c)$ should be. In the case of PrFeAsO_{1-y} , our measurements yield sufficient statistics for the expected increase of j_c with T_c to be, indeed, observed. In the considered portion of the phase diagram, the more vacancies are added, the higher T_c , but also the stronger the pinning. Fig. 10 shows a compilation of critical temperatures and low-temperature critical currents of all investigated regions in all our PrFeAsO_{1-y} crystals. The experimental data follow the dependence of the low temperature j_c as this follows from Eq. (5), even though this dependence is weak. The contribution to this dependence via n_d , arising from the addition of oxygen vacancies, is actually weaker than the expected contribution from the doping dependence of the the superfluid density, which we have assumed to follow the relation $\lambda^{-2} \propto T_c$.^{9,47} Significant scatter due to the strong pinning contribution remains in Fig. 10, which we shall attribute to the presence of doping inhomogeneity on the 10 – 100 nm scale

In the framework of weak collective pinning, the observed spatial variation of j_c in $\text{NdFeAsO}_{0.9}\text{F}_{0.1}$ would, if attributed to the macroscopic variation of the dopant atom density, correspond to a variation of the doping level of $x = 0.1 \pm 0.03$, within a given single crystal. The concomitant T_c variation would be from 26 K to nearly 50 K, which is not what is observed by DMO. Moreover, and contrary to the observation in PrFeAsO_{1-y} , the critical current density of the investigated crystal is larger in areas with low T_c , both as far as different regions of crystal # 1 are concerned, as the observed differences between crystals # 1 and 2. In the absence of sufficient statistics, we tentatively ascribe this behavior to the presence of strong background pinning.

C. Strong pinning background

As described in section III, the spatial variation of the critical current density in single crystalline PrFeAsO_{1-y} is reflected in the temperature dependence of j_c , higher local j_c corresponding to the presence of a break in the temperature dependence. Also, the higher local critical current densities are responsible for the low-field j_c -peak observed in Fig. 7, which cannot be explained within the single-vortex collective pinning framework. There must therefore be supplementary sources of pinning, inhomogeneously distributed throughout the samples, with a temperature dependence that is weaker than that of the weak collective pinning described above.

The field dependence of the associated critical current density, a plateau, followed by a power-law decrease $j_c \propto B^{-5/8}$, is in very satisfactory agreement with the theory of strong pinning developed in Refs. 43,48. In the presence of a density n_i of strong pins of size larger

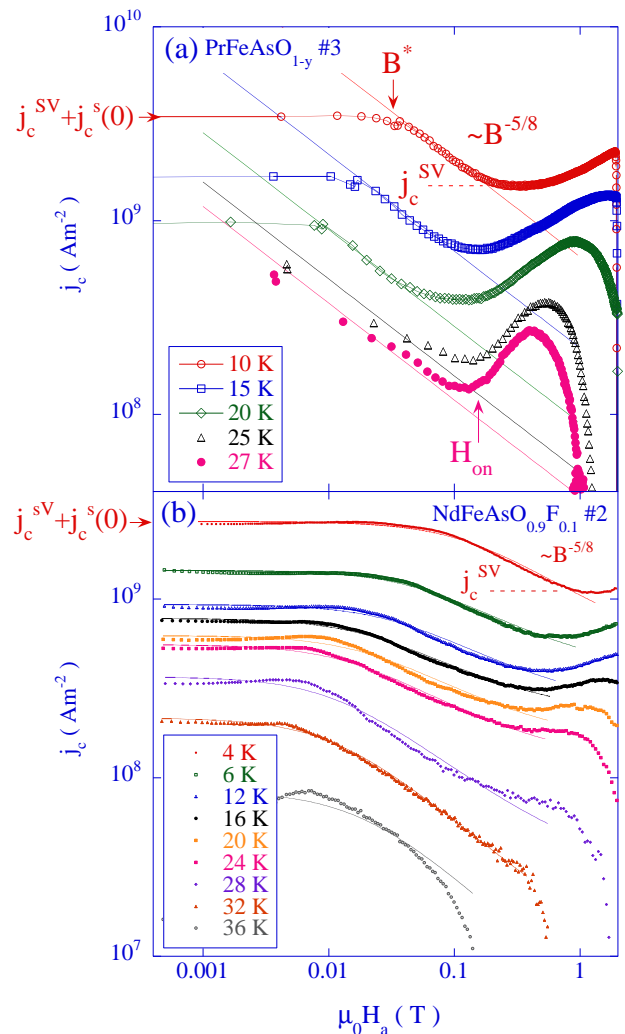


FIG. 11: (color online) (a) PrFeAsO_{1-y} : Double logarithmic plot of the critical current versus magnetic field. The drawn lines show the power $B^{-5/8}$ expected from the strong pinning contribution. (b) *ibid*, for $\text{NdFeAsO}_{0.9}\text{F}_{0.1}$. Drawn lines show model fits to Eq. 10.

than the coherence length, one has⁴³

$$j_c^s(0) = \frac{\pi^{1/2} n_i^{1/2} j_0}{\varepsilon_\lambda} \left(\frac{f_{p,s} \xi_{ab}}{\varepsilon_0} \right)^{3/2} (B < B^*) \quad (7)$$

$$j_c^s(B) \approx \frac{2n_i j_0}{\varepsilon_\lambda^{5/4} \xi_{ab}^{1/2}} \left(\frac{f_{p,s} \xi_{ab}}{\varepsilon_0} \right)^{9/4} \left(\frac{\Phi_0}{B} \right)^{5/8} (B > B^*). \quad (8)$$

The crossover field $B^* = 0.74 \varepsilon_\lambda^{-2} \Phi_0 (n_i / \xi_{ab})^{4/5} (f_{p,s} \xi_{ab} / \varepsilon_0)^{6/5}$ is determined as that above which the so-called vortex trapping area of a single pin is limited by intervortex interactions.⁴³ The identification of the experimental $j_c(0)$ with Eq. (7), and of the power-law decrease with Eq. (8), allows for the determination of the elementary pinning force $f_{p,s}$ of a strong pin from the ratio $[dj_c^s(B)/dB^{-5/8}] / [j_c^s(0)]^{-2}$. It

is found that $f_{p,s}(0) = 2 \times 10^{-13}$ N for both investigated compounds, with a temperature dependence coinciding with that of the superfluid density. Hence, we find a measured $f_{p,s} \sim 0.1\varepsilon_0$. The density of strong pins can be straightforwardly estimated from B^* : $n_i \approx 1 \times 10^{21}$ m⁻³ for PrFeAsO_{1-y}, and $n_i \approx 6 \times 10^{21}$ m⁻³ and $\approx 2 \times 10^{22}$ m⁻³ for NdFeAsO_{0.9}F_{0.1} crystals # 1 and 2, respectively.

These data can be compared to the results of TEM observations. The first candidate strong pins are extended (nm-sized) pointlike inclusions or precipitates, such as observed in Fig. 1b. Assuming such defects to be non-superconducting, one would have $f_{p,s} \sim \varepsilon_0 (D_i/4\xi_{ab}) \ln(1 + D_i^2/2\xi_{ab}^2)$. Typical observed defect dimensions are $D_i \approx 2 - 5$ nm, yielding $f_{p,s} \sim 0.1 - 1.1\varepsilon_0$ at low temperature. Therefore, the smaller defects of radius 2 nm might do the job, were it not that the temperature dependence expected for such voids is at odds with experiment.

Next, the observed undulations of the FeAs layers impose an intermittent bending of vortex lines as these move through the crystal lattice. The necessary force to produce this bending can be estimated as the product of the line tension $\varepsilon_\lambda^2 \varepsilon_0$ and the variance $(\delta\alpha)^2$ of the tilt angle; here, α corresponds to the buckling angle. Such a mechanism would yield the experimental temperature dependence of $f_{p,s}$, but, at $10^{-4}\varepsilon_0$, grossly underestimates the measured elementary force.

Third, the higher strong pinning critical current density observed for lower doped NdFeAs(O,F) could be linked to the observation of phase coexistence in the underdoped state of this material.⁹ Without going as far as invoking the presence of nm-scale magnetically ordered regions in our crystals, the idea of phase coexistence suggests that there are spatial fluctuations of the dopant atom density on the scale of several nm. The ensuing dispersion of weakly superconducting regions with critical temperature $T_c - \delta T_c$ inside a more strongly superconducting matrix would certainly lead to flux pinning. Its description would be similar to that of non-superconducting precipitates, but with a smaller pinning energy, a vortex passing through an area of lower T_c gaining only a fraction $\delta T_c/T_c$ of the condensation energy $\varepsilon_0/4\xi^2$. Assuming the condensation energy to be proportional to the critical temperature, the pinning force can be written as

$$f_{p,s} \approx \left[\varepsilon_0(t) - \left(1 - \frac{\delta T_c}{T_c}\right) \varepsilon_0(\tilde{t}) \right] \times \left(\frac{D_i}{4\xi_{ab}} \right) \ln \left(1 + \frac{D_i^2}{2\xi_{ab}^2} \right). \quad (9)$$

with $t \equiv T/T_c$, and $\tilde{t} \equiv T/(T_c - \delta T_c)$. For small spatial variations of the critical temperature, *e.g.* $\delta T_c/T_c \sim 0.05$ or $\delta T_c \approx 1.5$ K, and $D_i \sim 5 - 10$ nm, Eq. (9) nicely mimics the measured temperature dependence $f_{p,s}(T) \sim \varepsilon_0(T)$. As shown in Figs. 6, 9, and 11(b), the total critical current density, obtained by summing Eqs. (7) [with (9)

inserted] and (5),

$$j_c = j_c^{SV} + j_c^s. \quad (10)$$

is also in good agreement with experimental observations. One is thus led to the conclusion that, in addition to the macroscopic inhomogeneity of doping level, there also exists an inhomogeneity on the nano-scale, much similar to that reported by Yamamoto *et al.* in Ba(Fe_{0.9}Co_{0.1})₂As₂. However, the doping level modulation, necessarily of the order of the T_c -variation, $\delta T_c/T_c \sim 0.05$, that explains the strong pinning contribution, is far too small to support any claims of phase coexistence in the underdoped (1111) pnictides investigated here. If similar disorder should exist for smaller doping levels, near the superconductivity onset, one would have $\delta T_c \sim T_c$, and a near certain coexistence of magnetic and superconducting regions. This is a premise that needs further investigation.

For completeness, one may also contemplate surface roughness as a source of flux pinning.⁴⁹⁻⁵¹ The critical current density is then determined by the force needed to push a vortex line out of a surface trough or across a ridge, and reads, in the limit of small magnetic fields^{43,52}

$$j_c^{TV} = \frac{\pi\varepsilon_0}{\Phi_0 d} \frac{\delta d}{D} \quad \left(B \lesssim \frac{\Phi_0}{D^2} \right). \quad (11)$$

Here, d would be the crystal thickness, D the spacing between surface defects or troughs, and δd the typical ridge height, that is, the variance of the thickness. In Refs. 49-51, the ratio $\delta d/D = \sin \theta_c$ is interpreted as the sine of a ‘‘contact angle’’ θ_c . In the Mathieu-Simon model⁴⁹⁻⁵¹ the field dependence is expected to correspond to that of the vortex chemical potential, *i.e.* the equilibrium magnetization. This is not observed. Moreover, if one reinterprets the experimental $f_{p,s}$ and $n_i \sim 2/dD^2$ in terms of surface pinning, one finds a ratio of ridge height to ledge width $\delta d/D \sim 2$, for a ledge separation of ~ 20 nm. Such a high aspect ratio would mean that the surface defects are located on the crystal edge, since the alternative, cracks on the surface, are not observed. Strong pinning by impurities, located in surface regions only, leads to the same dependences (7,8), but with 3×10^{16} defects m⁻².

D. Fishtail effect and phase diagram

The knowledge of pinning parameters of the (1111) superconductors under study allows one to confront features of the mixed-state (B, T) -phase diagram with theoretical models. In particular, the fishtail effect at $B_{on}(T)$ was attributed to a crossover in vortex dynamics as, with increasing magnetic field, one leaves the single vortex pinning regime for the bundle pinning regime,^{53,54} or the occurrence of a first order phase transition from an ordered, ‘‘elastically pinned’’ low-field vortex phase, the so-called Bragg-glass,⁵⁵ to a high field disordered phase characterized by the presence of topological defects.^{56,57} The latter scenario has been unambiguously verified in

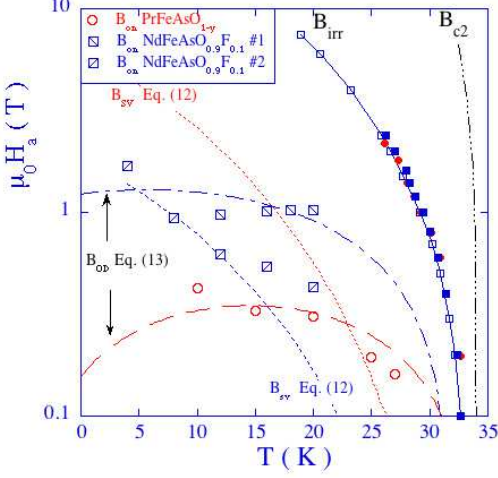


FIG. 12: (color online) (B, T) vortex matter phase diagram for (1111) iron pnictide superconductors. (Red) Circles indicate measurements on PrFeAsO_{1-y} , while (blue) squares show results on $\text{NdFeAsO}_{0.9}\text{F}_{0.1}$. Closed circles show the irreversibility field $B_{irr}(T)$ measured from the onset of a third harmonic reponse from ac Hall probe magnetometry; open (blue) squares show the screening onset data of Ref. 29. Peak effect onset fields for both compounds are indicated by barred squares ($\text{NdFeAsO}_{0.9}\text{F}_{0.1}$) and open (red) circles (PrFeAsO_{1-y}). Dotted lines show the single-vortex to bundle pinning crossover described by Eq. (12), while dashed-dotted lines indicate the order-disorder field described by Eq. (13).

the high temperature superconductors $\text{YBa}_2\text{Cu}_3\text{O}_{7-\delta}$ and $\text{Bi}_2\text{Sr}_2\text{CaCu}_2\text{O}_{8+\delta}$,¹⁷⁻¹⁹ in the cubic superconductor $(\text{Ba},\text{K})\text{BiO}_3$,⁵⁸ in NbSe_2 ,²⁰ as well as in MgB_2 .²¹

In the first case, the onset field B_{on} should coincide with the single-vortex- to bundle pinning crossover field B_{SV} , determined by the equality of R_c [see Eq. (3)] and the vortex spacing a_0 :

$$B_{SV} \sim 40B_{c2} \left(\frac{j_c^{SV}}{j_0} \right). \quad (12)$$

Inserting the experimentally obtained j_c^{SV} into Eq. (12) yields the dotted lines in Fig. 12. Clearly, while the experimental B_{on} data for more strongly pinning PrFeAsO_{1-y} lie below those for more weakly pinning $\text{NdFeAsO}_{0.9}\text{F}_{0.1}$, Eq. 12 predicts otherwise. Therefore, even if the peak effect onset lies in the vicinity of the single-vortex to bundle pinning crossover, it cannot be directly associated with it.

On the other hand, the vortex ensemble can undergo a structural transition whereby it lowers its energy by adapting itself more efficiently to the underlying pinning potential, at the expense of the generation of topological defects.⁵⁵⁻⁵⁷ In the absence of a theory for this order-disorder transition of the vortex lattice, a Lindemann-

like criterion was developed in Refs. 55,59 and 60 in order to, at least, estimate its position in the (B, T) -plane. The Lindemann approach considers that topological defects can be generated when pinning is sufficiently strong to provoke the wandering of vortex lines outside their confining cage formed by the nearest neighbor flux lines. The different results^{59,60} have been summarized in Ref. 57. In the regime of single vortex pinning, relevant for collective pinning in the (1111) compounds, the position of the order-disorder transition is given by

$$Ab_{SV}^{3/5}b_{OD}^{2/5} \left[1 + \frac{F_T(t)}{b_{SV}^{1/2}(1-b_{OD})^{3/2}} \right] = 2\pi c_L^2 \quad (13)$$

where $b_{on} \equiv B_{OD}/B_{c2}$, $b_{SV} = B_{SV}/B_{c2}$, $c_L \sim 0.1$ is the Lindeman number, A is a numerical constant, $t = t/T_c$, and $F_T(t) = 2t(Gi/1-t^2)^{1/2}$. The use of the parameters of Table I, the experimentally measured j_c^{SV} , and $A = 4$ yields the dashed lines in Fig. 12. These show more than satisfactory agreement with the experimentally measured positions of B_{on} . We therefore conclude that, most likely, a bulk order-disorder transition of the vortex lattice lies at the origin of the peak effect in (1111) pnictide superconductors. However, more work, especially on vortex dynamics and possible hysteresis associated with the transition, should be performed to ascertain this.

V. CONCLUSION

It is found that superconducting iron pnictide single crystals show significant spatial variations of both the critical temperature T_c and the critical current density j_c . Variations of these quantities on the macroscopic scale, from several to several hundred μm , are at the origin of a smearing of globally measured properties, and notably of the width of the superconducting transition. This implies the necessity of local measurements, such as magneto-optical imaging or Hall-probe magnetometry, to extract superconducting parameters. From such local measurements, it is found that the critical current in iron oxypnictide superconductors of the (1111) family of compounds arises from two distinct contributions. The first is weak collective pinning by dopant atoms or vacancies, vortex lines being pinned by the small scale fluctuations of the local dopant atom density. The pinning mechanism is identified as being due to mean-free path variations in the vortex core ($\delta\kappa$ mechanism). This means that dopant atoms should also be effective quasi-particle scatterers. The second pinning contribution manifests itself at low fields. The corresponding critical current contribution can be completely parametrized by the strong pinning theory developed in Refs. 43,48, which means that extended defects are at its origin. An analysis of the magnitude and field-dependence of this strong pinning contribution shows that spatial variations of the doping level on the scale of several dozen to one hundred nm may

be at stake. These variations do not support the possible coexistence of the anti-ferromagnetic metallic and the superconducting phases. Finally, we contend that a bulk order-disorder transition of the vortex ensemble is at the origin of the “fishtail” or peak effect observed in the critical current in sub-T fields.

Acknowledgements

We wish to acknowledge V. Mosser for providing the Hall sensor arrays. This work was supported by KAK-

ENHI from JSPS, and by Grant-in-Aid for the Global COE program “The Next Generation of Physics, Spun from Universality and Emergence” from MEXT, Japan. R.O. was supported by the JSPS Research Foundation for Young Scientists. Work at the Ames Laboratory was supported by the Department of Energy, Basic Energy Sciences under Contract No. DE-AC02-07CH11358.

-
- ¹ Y. Kamihara, H. Hiramatsu, M. Hirano, R. Kawamura, H. Yanagi, T. Kamiya, H. Hosono, *J. Am. Chem. Soc.* **128**, 10012 (2006).
- ² Y. Kamihara, T. Watanabe, M. Hirano, H. Hosono, *J. Am. Chem. Soc.* **130**, 3296 (2008).
- ³ Hiroki Takahashi, Kazumi Igawa, Kazunobu Arii, Yoichi Kamihara, Masahiro Hirano, and Hideo Hosono, *Nature* **453**, 376.
- ⁴ G.F. Chen, Z. Li, D. Wu, G. Li, W.Z. Hu, J. Dong, P. Zheng, J.L. Luo, and N.L. Wang, *Phys. Rev. Lett.* **100**, 247002 (2008).
- ⁵ Z.-A. Ren, J. Yang, W. Lu, W. Yi, G.-C. Che, X.L. Dong, L.-L. Sung, and Z.-X. Chao, *Mater. Res. Innovations* **12**, 105 (2008)
- ⁶ Ren Zhi-An, Lu Wei, Yang Jie, Yi Wei, Shen Xiao-Li, Zheng-Cai, Che Guang-Can, Dong Xiao-Li, Sun Li-Ling, Zhou Fang, and Zhao Zhong-Xian, *Chinese Phys. Lett.* **25** 2215-2216 (2008)
- ⁷ Hijiri Kito, Hiroshi Eisaki, and Akira Iyo, *J. Phys. Soc. Jpn.*, **77**, 063707 (2008).
- ⁸ M. Rotter, M. Tegel, and D. Johrendt, *Phys. Rev. Lett.* **101** 107006 (2008).
- ⁹ A.J. Drew, F.L. Pratt, T. Lancaster, S.J. Blundell, P.J. Baker, R.H. Liu, G. Wu, X.H. Chen, I. Watanabe, V.K. Malik, A. Dubroka, K.W. Kim, M. Rössle, and C. Bernhard, *Phys. Rev. Lett.* **101**, 097010 (2008).
- ¹⁰ D. Kubota, T. Ishida, M. Ishikado, S. Shamoto, H. Eisaki, H. Kito, A. Iyo, arXiv:0810.5623v1.
- ¹¹ R. Prozorov, N. Ni, M.A. Tanatar, V.G. Kogan, R.T. Gordon, C. Martin, E.C. Blomberg, P. Prommapan, J.Q. Yan, S.L. Bud’ko, and P.C. Canfield, *Phys. Rev. B* **78**, 224506 (2008).
- ¹² R. Prozorov, M.A. Tanatar, E.C. Blomberg, P. Prommapan, R.T. Gordon, N. Ni, S.L. Bud’ko, and P.C. Canfield, *Physica C* **469**, 667 (2009).
- ¹³ G. Blatter, M.V. Feigel’man, V.B. Geshkenbein, A.I. Larkin, and V.M. Vinokur, *Rev. Mod. Phys.* **66**, 1125 (1994).
- ¹⁴ Bing Shen, Peng Cheng, Zhaosheng Wang, Lei Fang, Cong Ren, Lei Shan, and Hai-Hu Wen, *Phys. Rev. B* **81**, 014503 (2010).
- ¹⁵ R. Prozorov, M. A. Tanatar, N. Ni, A. Kreyssig, S. Nandi, S. L. Bud’ko, A. I. Goldman, and P. C. Canfield, *Phys. Rev. B* **80**, 174517 (2009).
- ¹⁶ A. Yamamoto, J. Jaroszynski, C. Tarantini, L. Balicas, J. Jiang, A. Gurevich, D.C. Larbalestier, R. Jin, A.S. Sefat, M.A. McGuire, B.C. Sales, D.K. Christen, and D. Mandrus, *Appl. Phys. Lett.* **94**, 062511 (2009).
- ¹⁷ S. Kokkaliaris, P.A.J. de Groot, S.N. Gordeev, A.A. Zhukov, R. Gagnon, and L. Taillefer, *Phys. Rev. Lett.* **82**, 5116 (1999).
- ¹⁸ A.P. Rassau, S.N. Gordeev, P.A.J. de Groot, R. Gagnon, and L. Taillefer, *Physica C* **328**, 14 (1999).
- ¹⁹ C.J. van der Beek, S. Colson, M.V. Indenbom, and M. Konczykowski, *Phys. Rev. Lett.* **84**, 4196 (2000).
- ²⁰ S. Bhattacharya and M.J. Higgins, *Phys. Rev. Lett.* **70**, 2617 (1993); Y. Paltiel, E. Zeldov, Y.N. Myasoedov, H. Shtrikman, S. Bhattacharya, M.J. Higgins, Z.L. Xiao, E.Y. Andrei, P.L. Gammel, and D.J. Bishop, *Nature (London)* **403**, 398 (2000).
- ²¹ T. Klein, R. Marlaud, C. Marcenat, H. Cercellier, M. Konczykowski, C.J. van der Beek, V. Mosser, H.S. Lee, and S.I. Lee, submitted to *Phys. Rev. Lett.* (2009).
- ²² Huan Yang, Huiqian Luo, Zhaosheng Wang, and Hai-Hu Wen, *Appl. Phys. Lett.* **93**, 142506 (2008).
- ²³ Huan Yang, Cong Ren, Lei Shan, and Hai-Hu Wen, *Phys. Rev. B* **78**, 092504 (2008).
- ²⁴ R. Prozorov, M. E. Tillman, E. D. Mun, P.C. Canfield, *New Journal of Physics* **11**, 035004 (2009).
- ²⁵ X.L. Wang, S.R. Ghorbani, S.X. Dou, X.L. Shen, W. Yi, Z.C. Li, and Z.A. Ren, arXiv:0806.1318v1.
- ²⁶ M. Ishikado, S. Shamoto, H. Kito, A. Iyo, H. Eisaki, T. Ito, and Y. Tomioka, *Physica C* **469**, 901 (2009).
- ²⁷ R. Okazaki, M. Konczykowski, C.J. van der Beek, T. Kato, K. Hashimoto, M. Shimozawa, H. Shishido, M. Yamashita, M. Ishikado, H. Kito, A. Iyo, H. Eisaki, S. Shamoto, T. Shibauchi, and Y. Matsuda, *Phys. Rev. B* **79**, 064520 (2009).
- ²⁸ K. Hashimoto, T. Shibauchi, T. Kato, K. Ikada, R. Okazaki, H. Shishido, M. Ishikado, H. Kito, A. Iyo, H. Eisaki, S. Shamoto, and Y. Matsuda, *Phys. Rev. Lett.* **102**, 017002 (2009).
- ²⁹ J. Kacmarcik, C. Marcenat, T. Klein, Z. Pribulova, C.J. van der Beek, M. Konczykowski, S.L. Bud’ko, M. Tillman, N. Ni, and P.C. Canfield, *Phys. Rev. B* **80**, 014515 (2009).
- ³⁰ Z. Pribulova, T. Klein, J. Kacmarcik, C. Marcenat, M. Konczykowski, S. L. Bud’ko, M. Tillman, and P. C. Canfield, *Phys. Rev. B* **79**, 020508(R) (2009).
- ³¹ L.A. Dorosinskiĭ, M.V. Indenbom, V.I. Nikitenko, Yu.A. Ossip’yan, A.A. Polyanskiĭ, and V.K. Vlasko-Vlasov, *Physica C* **203**, 149 (1992).
- ³² A. Soibel, E. Zeldov, M.L. Rappaport, Y. Myasoedov, T.

- Tamegai, S. Ooi, M. Konczykowski, and V. Geshkenbein, *Nature* **406**, 282 (2000).
- ³³ E.H. Brandt, *Phys. Rev. B* **54**, 4246 (1996).
- ³⁴ T. Shibauchi, M. Konczykowski, C.J. van der Beek, R. Okazaki, Y. Matsuda, J. Yamaura, Y. Nagao, and Z. Hiroi, *Phys. Rev. Lett.* **99**, 257001 (2007).
- ³⁵ C.P. Bean, *Phys. Rev. Lett.* **8**, 250 (1962)
- ³⁶ E.H. Brandt, M.V. Indenbom and A. Forkl, *Europhys.Lett.* **22**, 735 (1993).
- ³⁷ E. Zeldov, J.R. Clem, M. McElfresh, and M. Darwin, *Phys. Rev. B* **49**, 9802 (1994).
- ³⁸ C.J. van der Beek, M. Konczykowski, V.M. Vinokur, G.W. Crabtree, T.W. Li, and P.H. Kes, *Phys. Rev. B* **51**, 15492 (1995).
- ³⁹ A.I. Larkin and Yu. N. Ovchinnikov, *J. Low Temp. Phys.* **21**, 409 (1979).
- ⁴⁰ G. Blatter et V.B. Geshkenbein, *Vortex Matter*, in "Superconductivity. Conventional and Unconventional Superconductors Vol. 1", pp 495-625, Ed. K. Bennemann et J.B. Ketterson, Springer, Berlin (2008).
- ⁴¹ E. H. Brandt, *Phys. Rev. Lett.* **57**, 1347 (1986).
- ⁴² E.V. Thuneberg, J. K urkij arvi, and D. Rainer, *Phys. Rev. Lett.* **48**, 1853 (1982); *Phys. Rev. B* **29**, 3913 (1984).
- ⁴³ C.J. van der Beek, M. Konczykowski, A. Abal'oshev, I. Abal'osheva, P. Gierlowski, S.J. Lewandowski, M.V. Indenbom, S. Barbanera, *Phys. Rev. B* **66**, 024523 (2002).
- ⁴⁴ The different temperature dependences arise from the different temperature dependence of ε_λ in the two compounds; Whereas ε_λ increases with temperature in PrFeAsO_{1-y} it is nearly temperature independent in $\text{NdFeAs}_{0.9}\text{F}_{0.1}$.
- ⁴⁵ C.R. Rotundu, D.T. Keane, B. Freelon, S.D. Wilson, A. Kim, P.N. Valdivia, E. Bourret-Courchesne, and R.J. Birgeneau, arXiv:0907:1308v1.
- ⁴⁶ G. F. Chen, Z. Li, D. Wu, J. Dong, G. Li, W. Z. Hu, P. Zheng, J. L. Luo, and N. L. Wang, *Chin. Phys. Lett.* **25**, 2235 (2008) .
- ⁴⁷ Y.J. Uemura, G.M. Luke, B.J. Sternlieb, J.H. Brewer, J.F. Carolan, W.N. Hardy, R. Kadono, J.R. Kempton, R.F. Kiefl, S.R. Kreitzman, P. Mulhern, T.M. Riseman, D.L. Williams, B.X. Yang, S. Uchida, H. Takagi, J. Gopalakrishnan, A.W. Sleight, M.A. Subramanian, C.L. Chien, M.Z. Cieplak, G. Xiao, V.Y. Lee, B.W. Statt, C.E. Stronach, W.J. Kossler, X.H. Yu, *Phys. Rev. Lett.* **62**, 2317 (1989).
- ⁴⁸ Yu. N. Ovchinnikov and B.I. Ivlev, *Phys. Rev. B* **43**, 8024 (1991).
- ⁴⁹ P. Mathieu and Y. Simon, *Europhys. Lett.* **5**, 67 (1988).
- ⁵⁰ Y. Simon, B. Pla ais, and P. Mathieu, *Phys. Rev. B* **50**, 3503 (1994).
- ⁵¹ G. Lazard, P. Mathieu, B. Pla ais, J. Mosqueira, Y. Simon, C. Guilpin and G. Vaquier, *Phys. Rev. B* **65**, 064518 (2002).
- ⁵² R.B. Flippen, T.R. Askew, J.A. Fendrich, and C.J. van der Beek, *Phys. Rev. B* **52**, R9882 (1995).
- ⁵³ L. Krusin-Elbaum, L. Civale, V.M. Vinokur, F. Holtzberg, *Phys. Rev. Lett.* **69**, 2280 (1992).
- ⁵⁴ L. Civale, L. Krusin-Elbaum, J.R. Thompson, and F. Holtzberg, *Phys. Rev. B* **50**, 7188 (1994).
- ⁵⁵ T. Giamarchi and P. Le Doussal, *Phys. Rev. B* **55**, 6577 (1997).
- ⁵⁶ J. Kierfeld and V.M. Vinokur, *Phys. Rev.* **61**, R14928 (2000); *ibid.* **69**, 024501 (2004).
- ⁵⁷ G.P. Mikitik and E.H. Brandt, *Phys. Rev. B* **64**, 184514 (2001); *ibid* *Phys. Rev. B*, **68**, 054509 (2003); *ibid* *Phys. Rev. B*, **71**, 012510 (2005).
- ⁵⁸ T. Klein, I. Joumard, S. Blanchard, J. Marcus, R. Cubitt, T. Giamarchi, P. Le Doussal, *Nature (London)* **413**, 404 (2001).
- ⁵⁹ D. Ertaş and D.R. Nelson, *Physica C* **272**, 79 (1996).
- ⁶⁰ V.M. Vinokur, B. Khaykovich, E. Zeldov, M. Konczykowski, R.A. Doyle, and P.H. Kes, *Physica C* **295**, 209 (1998).